Relativistic cyclotron resonance condition as applied to Type II interplanetary radio emission

William M. Farrell, Michael L. Kaiser, Stuart D. Bale, M. D. Desch, R. J. Fitzenreiter, Keith Goetz, Jean-Louis Bougeret

Relativistic cyclotron resonance condition as applied to Type II interplanetary radio emission

W. M. Farrell,[1] M. L. Kaiser,[1] S. D. Bale,[2] M. D. Desch,[1] R. J. Fitzenreiter,[1] K. Goetz,[3] and J.-L. Bougeret[4]

Received 3 April 2003; revised 14 August 2003; accepted 4 September 2003; published 10 February 2004.

[1] We demonstrate that energy from energetic electrons upstream of interplanetary (IP) shocks are able to couple directly to the o-mode radio branch via the relativistic cyclotron harmonic resonance interaction, thereby creating the Type II radiation observed from IP shocks. The conditions required for the electron/wave resonance are that the wave frequency, f, lies near the local plasma frequency, f_p, and near (but not exactly at) the cyclotron harmonics, mf_c, where m is the cyclotron harmonic number. We compare the details of this relativistic electron cyclotron harmonic theory with observations in a Type II source region, with good agreement in many areas including the prediction of "Zeeman" splitting of the Type II emission. Based on the character of the high-resolution emission spectrum, we can narrow the Type II source location to the IP shock foot region and place some general conditions on shock topology required for Type II emission. *INDEX TERMS:* 7534 Solar Physics, Astrophysics, and Astronomy: Radio emissions; 7847 Space Plasma Physics: Radiation processes; 7867 Space Plasma Physics: Wave/particle interactions; 7871 Space Plasma Physics: Waves and instabilities; 7851 Space Plasma Physics: Shock waves; *KEYWORDS:* solar type II emission, solar physics, plasma instabilities

Citation: Farrell, W. M., M. L. Kaiser, S. D. Bale, M. D. Desch, R. J. Fitzenreiter, K. Goetz, and J.-L. Bougeret (2004), Relativistic cyclotron resonance condition as applied to Type II interplanetary radio emission, *J. Geophys. Res.*, *109*, A02106, doi:10.1029/2003JA009965.

1. Introduction

[2] Interplanetary Type II radio emission has become a recognized signature of incoming solar-originating coronal mass ejections (CMEs). The emission is emitted from the front (upstream) of IP shocks associated with the CME at the local f_p (and 2 f_p) [*Cane et al.*, 1981]. The emission frequency is thus indicative of the shock location and eventual arrival at Earth. While the utilization of Type II emission as a diagnostic tool of IP shock location has increased, the fundamental understanding of the Type II emission process still remains the subject of considerable debate. In this work, we will examine the relativistic cyclotron resonance condition and in particular demonstrate the ability of energetic electrons at the shock to couple directly with the o-mode escaping radio branch in the IP medium via electron cyclotron harmonic (ECH) emission.

[3] Direct coupling of IP energetic electrons to the o-mode was previously not considered likely. Specifically, in a high-density solar wind, with $f_p \gg f_c$, the resonance condition is approximated to the Cerenkov condition: $\omega - k_{\|}v_{\|res} = 0$. The electron resonance velocity for this condition is $v_{\|res} = c/n_{\|}$, which for coupling to the o-mode branch (with $n_{\|} < 1$) requires electron velocities greater than the speed of light. Consequently, other mechanisms for coupling were developed.

[4] The initial modeling of Type II emission took a parallel track to the more mature modeling of Type III radio emission [*Nelson and Melrose*, 1985], with the consideration of large k-valued beam-generated Langmuir wave-wave interactions coupling to the small k-valued o-mode branch. The underlying approach to such wave-wave models is to find a way to convert energetic electron energy into large k-valued electrostatic waves and then to down-convert the energy to small k-values that are consistent with the o-mode branch.

[5] Recently, *Farrell* [2001] demonstrated that when the relativistic cyclotron resonance condition is considered in full, high-ordered electron cyclotron harmonic emission can have very low wave phase speeds (at frequencies near each of the electron cyclotron harmonics). These low wave phase speeds allow a resonance with mildly energetic suprathermal electrons found at IP shocks. Further, the growth rate of the instability is functionally dependent on the Bessel Function, $J_m(k_{\perp}v_{\perp}/\omega_c)$, and this quantity becomes large when its argument is large. The growth rate is also dependent on the presence of a positive slope in the electron perpendicular distribution: $df/dv_{\perp} > 0$. It was thus demonstrated that direct coupling to the o-mode, near f_p, is possible, in general, for cases of a mildly energetic

[1]Laboratory for Extraterrestrial Physics, NASA Goddard Space Fight Center, Greenbelt, Maryland, USA.
[2]Space Science Laboratory, University of California, Berkeley, Berkeley, California, USA.
[3]School of Physics and Astronomy, University of Minnesota, Minneapolis, Minnesota, USA.
[4]Departement de Recherche Spatiale, Observatoire de Paris, Meudon, France.

0148-0227/04/2003JA009965

gyrotropic electron beam. Consequently, the requirement for wave-wave interactions can be relaxed or removed altogether.

[6] In this work, we will focus on the cyclotron resonance condition itself, demonstrating the direct electron/o-mode coupling during the Wind spacecraft passage through an IP shock and Type II source region where energetic electrons are also observed [*Bale et al.*, 1999]. While the previous presentation [*Farrell*, 2001] emphasized the overall general stability of the ECH emission, this work will re-present the analysis emphasizing the resonant index of refractions in a more illustrative demonstration of the electron/wave coupling process.

2. ECH Resonance Condition and Resonant Velocity

[7] The complete electron cyclotron resonance condition with relativistic effects is

$$\omega - k_{\|} v_{\|res} = m\omega_c \gamma^{-1}, \quad (1)$$

which can be reexpressed (with $\gamma^{-1} \sim (1 - v^2/2c^2)$) as

$$n^m_{res} = A(1 - Y_m(1 - B)), \quad (2)$$

where $A = c/v_{\|} \cos\theta$, $Y_m = mf_c/f$, $B = v^2/2c^2$. The variable θ is the wave normal angle and m is the order of the cyclotron harmonic.

[8] Figure 1 illustrates the resonance condition for $f > f_p$ defined by equation (2) for $f_p = 27.8$ kHz and $f_c \sim 300$ Hz. These chosen values are consistent with the conditions in a Type II source region described by *Bale et al.* [1999]. Specifically, we will define m_o as the first viable ECH above f_p, $m_o \geq f_p/f_c \sim 90$. In the dense solar wind, the value of m_o is typically large. Note that for each n^m_{res}, a zero exists at $f = (1 - B)\, m\, f_c$, and the slope of the resonant index is $dn^m_{res}/df \sim mf_cA\,(1 - B)/f^2$.

[9] For large wave normal angles (consistent with the o-mode) and mildly energetic electrons ($v/c \sim 0.01$–0.1), the resonant index for each harmonic, n^m_{res}, has a very steep slope (almost vertical on an n vs f plot) with an origin near but very slightly downshifted from each mf_c. In Figure 1, $\theta = 89°$, $v_{\perp} \sim 0.1\, v_{\|}$ and $v_{\|}/c \sim 0.01$ are applied. In essence, for very oblique wave normal angles and electron velocities below 10 keV, the curves appear generically like the steeped sloped versions presented in Figure 1. As $v_{\|}$ approaches zero, the slope of the index approaches infinity.

[10] Consider now the resonant index for the m-th ECH, n^m_{res}, and wave frequencies very near mf_c. Under these circumstances, $f \sim mf_c$, $Y_m \cong 1$ and $B = v_{\|}^2/2c^2 + v_{\perp}^2/2c^2$, making equation (2) a most interesting form:

$$n^m_{res} = (2\cos\theta)^{-1}\left[(v_{\|}/c) + (v_{\perp}/v_{\|})(v_{\perp}/c)\right]. \quad (3)$$

Because the curve of n^m_{res} is very steep, much of the curve fits the condition that $Y_m \cong 1$, making equation (3) applicable at most points along each of the curves in Figure 1. In essence, each of the curves in Figure 1 is so steep as to be nearly independent of frequency (i.e., for each defined value of m, they exist essentially at a single frequency). As implied in Figure 1, resonance occurs between the waves and electrons at points where $n^m_{res} = n_{omode}$. These locations are indicated in the figure (i.e., thick dots). At these locations, equation (3) is equal to the o-mode index of refraction, and we thus obtain:

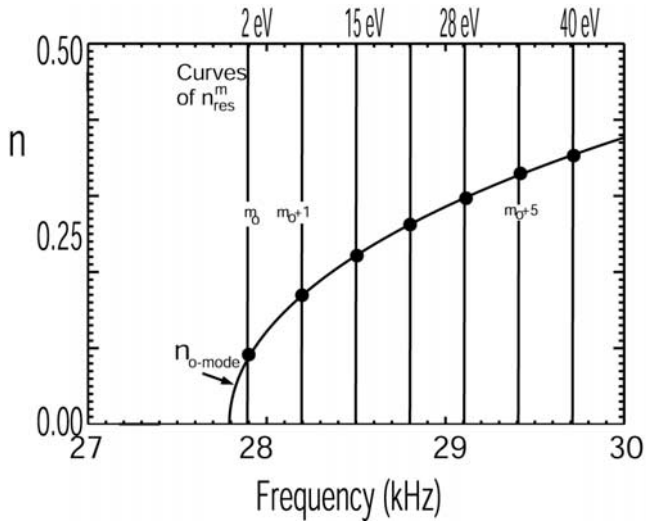

Figure 1. The index of refraction associated with relativistic electron cyclotron harmonic condition, overlaid on the o-mode index. Note that intersections of the two occur at regularly spaced intervals in frequency. Electrons will exchange free energy to the waves at these resonance locations. The associated electron energy is labeled at the top of the figure.

$$(2\cos\theta)^{-1}\left[(v_{\|}/c) + (v_{\perp}/v_{\|})(v_{\perp}/c)\right] = (1 - X)^{1/2}, \quad (4)$$

where $n_{omode} = (1 - X)^{1/2}$ and $X = f_p^2/f^2$. As suggested by Figure 2 of *Bale et al.* [1999], the Type II source region upstream of IP shocks has $v_{\|} \gg v_{\perp}$. We can thus derive an approximate expression for the parallel resonant electron velocity for each ECH at locations where $n^{mo}_{res} = n_{omode}$:

$$v_{\|res} \sim 2\, c\, \cos\theta(1 - X)^{1/2}. \quad (5)$$

The top of Figure 1 includes the associated resonant energy ($m_e v_{\|res}^2/2e$) associated with the mode/resonance interception points as defined by equation (5), assuming a wave normal angle of 89°. Note that the resonant energy steadily increases with increasing ECH number above f_p. A specific energy also will excite a specific ECH. For example, an anisotropic electron beam with narrow energy near 15 eV will excite the $m_o + 2$ mode while a similar beam near 40 eV will excite the higher-frequency $m_o + 6$ mode.

[11] It is thus evident that moderately energetic electrons can indeed directly interact with o-mode waves near the local plasma frequency via the relativistic electron cyclotron harmonic resonance. Equation (5) can only be realized by including the relativistic terms in the resonance condition. Without relativistic terms, the velocity dependence on $(1 - X)^{1/2}$ is inverse rather than direct.

[12] Equation (5), describing the parallel resonance velocity, can be compared with the unapproximated resonant

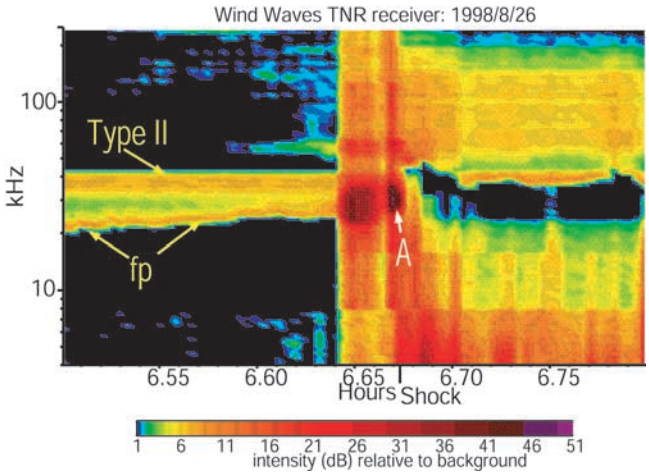

Figure 2. A Wind/WAVES spectrogram during a passage of an IP shock. Note that the local Langmuir wave activity increases by almost 30 dB at point A. Also note the presence of the Type II emission between 32 and 42 kHz.

velocity condition defined in equation (15) in the work of *Farrell* [2001]. In its full form, the resonant velocity forms an ellipse in phase space with ellipse center, v_c, lying on the $v_{||}$ axis with ellipse intercepts at $v_c + v_{ma}$ and $v_c - v_{ma}$, with v_{ma} being the ellipse semimajor axis. The variable $v_c = B/A$ and $v_{ma} = D/Y_m$, where $A = (Y_m^2 + n^2\cos\theta^2)^{1/2}$, $B = cn\cos\theta/A$, and $D = (c^2(Y_m^2 - 1) + B^2)^{1/2}$. For $Y_m \sim 1$ and $n\cos\theta \ll 1$, it is easy to demonstrate that $v_c \sim v_{ma} \sim cn\cos\theta \sim c\cos\theta(1 - X)^{1/2}$. Consequently, the value of equation (5) is comparable to being located at the ellipse/$v_{||}$ axis intercept at $v_c + v_{ma}$, corresponding to the ellipse's most energetic parallel point. As such, equation (5) above represents the upper bound to the possible parallel velocities and represents a good indicator for the ellipse location in phase space, particularly near the $v_{||}$ axis.

3. Observations at a Type II Source Region

[13] *Bale et al.* [1999] reported on the Wind spacecraft passage directly through an IP shock and Type II generation region, this occurring on 26 August 1998 at 0640:19 UT. Their Figure 2 presents Wind WAVES [*Bougeret et al.*, 1995], 3DP particle [*Lin et al.*, 1995] and MFI magnetic field [*Lepping et al.*, 1995] measurements. Specifically, for the 5-min period preceding the shock, the IP medium was relatively calm maintaining a particle density of 7/cm^3 and magnetic field strength of ~7–9 nT, corresponding to $f_p \sim$ 24–28 kHz and f_c of ~200 Hz. Near 0640:15 UT, a steep ramp-up in magnetic field and plasma density was observed, the former varying from 9 to 25 nT and the latter from 7 to 27 el/cm^3 in <30 s.

[14] *Bale et al.* [1999] also display (their Figure 2) the electron flux between 23 and 1140 eV in the parallel, antiparallel, and perpendicular directions to the ambient magnetic field. As illustrated in their figure, a significant parallel and antiparallel electron flux above 70 eV was observed from 0638 UT to 0640:30 UT, preceding the shock by a few minutes. This electron flux occurred in direct association with an enhanced f_p electrostatic emission. *Bale et al.* [1999] rightly conclude that the energetic electron flow and f_p emission signature preceding the shock is consistent with the spacecraft passage though an IP foreshock. Since the Type II emission is observed continuously for hours preceding the shock, ceaselessly to the shock front, they further conclude that the spacecraft was in the near-vicinity of a Type II source region.

[15] Specifically, Figure 2 shows a Wind/WAVES spectrogram from the Thermal Noise Receiver (TNR) [*Bougeret et al.*, 1995] for a 1/2 hour period approximately centered about the shock at 0640:19 UT on 26 August 1998 (shock indicated on figure). The local plasma frequency (as identified by the thermal noise) is labeled on the figure. Type II emission is indicated in the figure, extending from 0630 to 0640 UT, in a broad band between 32 and 42 kHz.

[16] Note that at 0630 UT the local plasma frequency is 20 kHz but gradually increases to nearly 30 kHz as the spacecraft approaches the shock. At 0640 UT (or 6.67 hours), an intense burst of emission at f_p, nearly ~47 dB above the noise level, is observed near 30 kHz, occurring at the base of the shock ramp. This intensification, labeled "A" in the figure, is in the electron foreshock region previously identified by *Bale et al.* [1999]. By 0642 UT, the spacecraft is behind the shock and the local plasma frequency is ~50 kHz.

[17] Unfortunately, the TNR does not possess the spectral resolution to resolve the desired details in the Type II spectra. However, Wind/WAVES also has a Time Domain Sampler (TDS) [*Bougeret et al.*, 1995] capable of capturing a 17 ms waveform snapshot at 120 k Samples/s in a 60 kHz bandpass. The snapshot is triggered based on intensity. The system fortuitously captured the intense f_p emission occurring at 0640:10 UT (point A in Figure 2).

[18] Figure 3 displays spectra from the Ex and Ey antennae at 0640:10 UT. The spectra are created via Fourier Transform of the 2000 point high-rate waveform. The spectra are smoothed (2 point smoothing) to give an approximately 100 Hz spectral resolution. The strongest signal is the obvious peak at 27.8 kHz: the intense emission at f_p. The emission has a power of nearly −30 dB, corresponding to waveform amplitudes of ±40 mV/m. The emission has a

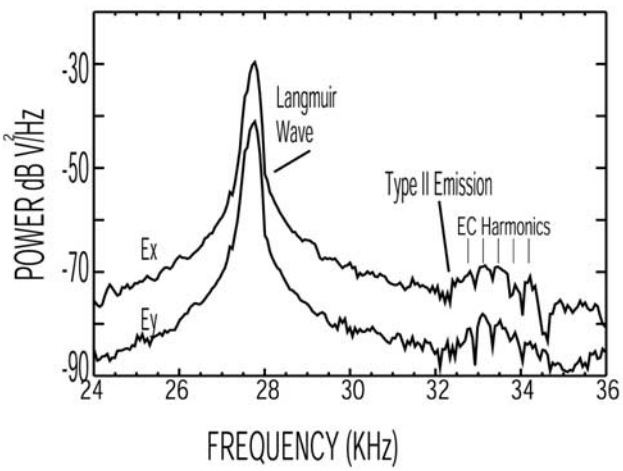

Figure 3. The high-resolution spectra of the wave activity at Point A in Figure 2. Note the observation of the Type II emission and associated electron cyclotron harmonics.

narrow intrinsic bandwidth of about 300 Hz, measured at 10% of peak power. The plasma frequency corresponds to a density of 9–10/cm^3 and based on Figure 2g of *Bale et al.* [1999] is consistent with being at the base of the shock ramp (at the end of the foreshock region).

[19] A most interesting signal captured by the TDS is the relatively weak emission between 32 and 35 kHz, this being the IP Type II emission. The high rate waveforms of this event are the first of their kind, allowing an examination of the emission at the Nyquist frequency. A digitization noise analysis is discussed in Appendix A, demonstrating that the emission is not associated with TDS sampling noise. Typically, the detection of IP Type II emission requires a sensitive receiver with relatively large integration times to increase the signal-to-noise level of the intrinsically weak, remotely sensed emission. The ability to capture a well defined high-resolution emission spectra for the Type II emission on 26 August 1998 is due to being in the vicinity of the Type II source region. Note that the emission is much broader than the more intense f_p emission, with a 1.2 kHz bandwidth. The emission is also upshifted by about 5kHz (~20%) relative to the intense emission at f_p, making its frequency of occurrence at $f \sim 1.2–1.3\ f_p$. As we demonstrate in section 4, this 20–30% upshift is explainable via the ECH mechanism. Finally, the emission appears to have discrete frequency fine structure overlaid on the diffuse, broadband emission. This fine structure appears to be modulated near ~300 Hz, consistent with a magnetic field magnitude of ~11 nT. This magnetic field value is associated with a location about 1/4 of the way up the fast-ramping portion of the shock magnetic field. We thus further localize the source of the Type II emission to the earliest portion of the shock ramp, at the backend of the foreshock region identified by *Bale et al.* [1999]. Thus using the electron cyclotron harmonic splitting, we are able to define the source location of the Type II emission in a way that has not been presented previously.

[20] We elaborate on the Type II source location further. We state that the source is located in the foreshock region just adjacent to the shock itself. According to Figure 2h of *Bale et al.* [1999], the 300 Hz (11 nT) cyclotron splitting of the emission places the location about 1/4 of the way up the magnetic shock ramp signature. As suggested by Bale et al.'s Figure 2g, the associated density signature has yet to show any shock ramping at this exact time and location. The local f_p emission at 27.8 kHz (obtained via Figure 3) indicates a local density of ~9 el/cc, consistent with the source being just at the foot of the shock but still in preshocked plasma. We conclude that the magnetic field initiates ramping before the density. The early magnetic ramp has the classic appearance of an extended shock "foot" created by reflected ions (see Figure 3.9 of *Tidman and Krall* [1971]). Such a foot would be evident in a quasi-perpendicular shock like the one encountered. The emission source appears to lie in this magnetic-extended foot region where electrons are observed to have increased perpendicular momentum.

[21] The observed cyclotron splitting is predicted by the emission model via the cyclotron harmonic maser instability (see section 2). This Type II electron cyclotron harmonic structure ("Zeeman" splitting) has some distinct similarities to the electron cyclotron and 1/2 cyclotron band splitting fine structure of radiated f_p emission observed from the terrestrial shock region [*Cairns*, 1986]. These terrestrial f_p emissions are considered as the analog to the Type II emission. The fact that both have similar electron cyclotron-related fine structure suggests that similar processes are occurring in both types of shocks. As stated in the work of *Cairns* [1986], the current wave-wave theories have difficulty explaining these ECH-related structures. Another example of this Type II cyclotron splitting is shown in Appendix B.

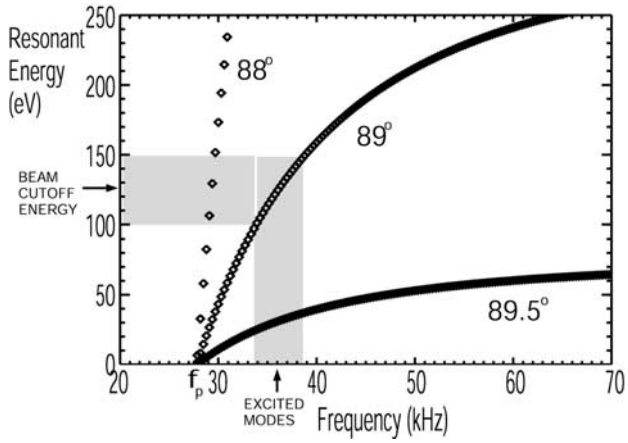

Figure 4. Using the resonance velocity in equation (5) and the conditions observed in the IP shock ramp on 26 August 1998 at 0640:19 UT, we have derived the electron resonant energy dependence with frequency. Note that the observed 3DP beam cutoff between 100 and 150 eV is consistent with the generation of a number of ECH modes between 30 and 40 kHz, much like the observations in Figure 3.

4. Integration of Theory and Observation

[22] *Bale et al.*'s [1999] Figure 2 indicates the presence of antiparallel (outward flowing) energetic electrons preceding the shock by ~2 min. There is also the presence of a second parallel (inward flowing) component preceding the shock by ~20 s. As described therein, the electron distribution has been identified as foreshock-like, with the low-energy electron beam cutoff [*Fitzenteiter et al.*, 1990] between 100 and 150 eV. This beam cutoff region is typically the source location of wave free energy, with distributions possessing positive slopes near the cutoff energy [*Fitzenteiter et al.*, 1990].

[23] Figure 4 displays the resonant energy (via equation (5)) as a function of frequency for $f_p = 27.8$ kHz and $f_c = 300$ Hz, consistent with the plasma environment at 0640:10 UT. Various wave normal angles are included. The diamonds indicate the approximate frequency for each of the ECHs. Note that as the wave frequencies approach the local plasma frequency, the resonant energy progressively decreases allowing low-energy electrons to interact directly with the waves. Again, this trend in resonant energy versus frequency is only realized by keeping the relativistic terms in the resonance condition.

[24] Given the cutoff beam energy between 100 and 150 eV and the assumption that an electron anisotropy exists near the cutoff energy, we find that the electrons in proximity of the cutoff energy can excite a number of ECH

modes between 33 and 39 kHz. We highlight the range of indices excited by the foreshock electron anisotropy in the figure.

[25] In examining Figure 3, we note that there is a distinct frequency upshift of the o-mode Type II emission relative to the local f_p of about 5 kHz ($f \sim 1.2-1.3\ f_p$). This upshift is associated with the detailed energy of the exciting suprathermal electrons, with this frequency separation progressively decreasing with decreasing electron beam energy. Thus we conclude that the emission is not generated at f_p or $2\ f_p$ but at a frequency consistent with the details of the electron distribution, about 1/4 of the way between these two characteristic frequencies. We also note that this beam should excite specific modes with distinct enhancements spaced by the electron cyclotron frequency (harmonically spaced fine structure). This fine structure is consistent with the Type II observations in Figure 3.

[26] We note from Figure 4 that assumed wave normal angles other than 89° yield very different emission configurations. The angle of 89° was chosen in part because the results fit the observations. However, the angle applied is an assumption and as such makes the theoretical analysis mathematically nonunique. The observations of ECH (Figure 3 and Appendix B) stand on their own merit as a unique observation. The model and interpretation, while being as consistent as possible to the observations, is considered inherently nonunique. We understand that while we have successfully demonstrated the applicability of the ECH model to the observations, other investigators may have other equally valid explanations that may fit the observations.

5. Conclusions

[27] A number of new scientific findings have been presented: First, high-resolution (~100 Hz) spectra of Type II emission in their source region are presented for the first time. Second, we find an observed upshift of the Type II emission frequency from the local plasma frequency by 20–30% in the source region. Third, ECH fine structure is observed overlaying the Type II emission. This fine structure is observable only via high-resolution waveform data. Fourth, we further localize the Type II source to the foot portion of the shock magnetic field. Finally, a possible theory involving ECH emission is presented to place the observations in context. Typically, Type II emission sensed remotely is very weak and not capable of detection via the Wind WAVES Time Domain Sampling system. However, Wind fortuitously flew in/near the Type II source region where emission strengths are the largest, thereby allowing the emission capture via the waveform system. Another fortuitous case is shown in Appendix B.

[28] Regarding the emission source region, we note that energetic electrons are observed throughout the foreshock region, yet the Type II emission appears to originate from the foot region at the base of the shock. We thus ask the question: Why is Type II emission apparently limited to the shock foot? What element of the foot triggers the emission mechanism? There are two possible explanations. First, in this "near-shock" foot region, newly created outflowing foreshock electrons possess large amounts of free energy and hence radiate intensely in a number of modes, including radiative ECH and Langmuir waves.

[29] However, a second possibility suggests that free energy can be created as inflowing electrons enter the foot. Specifically, *Farrell* [2001] demonstrated that ECH wave growth requires the Bessel function (and its argument) $J_m(k_\perp v_\perp/\omega_c)$ to be large and that $df/dv_\perp > 0$. Both of these functions are included in the kernel of the growth rate integral. As described by *Bale et al.* [1999], the IP foreshock suprathermal electrons possess primarily B-parallel and B-antiparallel flow and little perpendicular momentum. Thus J_m is small and $df/dv_\perp < 0$. However, in the shock ramp where B is steadily increasing, the electron pitch angle for the inward flowing electrons should also increase, thereby giving this suprathermal electron component increasing perpendicular momentum as it moves inward towards the shock center. Thus J_m should progressively increase as the inward propagating beam moves through the shock foot. Given conservation of particle energy, this increasing perpendicular momentum is at the expense of parallel momentum, yielding distributions smeared along constant pitch angle as the initially narrow beam moves through the ramp. Thus the electron distributions in the ramp now possess $df/dv_\perp > 0$. As a result of the inward beam's movement into the ramp, the two conditions required for wave growth are now met. Note that this argument only applies to the energetic electron component moving inward toward the shock.

[30] If this scenario is true, we could infer that a critical ingredient for Type II generation at an IP shock is energetic electrons flowing into the shock itself, and this condition is a function of the specific shock geometry. As demonstrated by *Bale et al.* [1999], a shock front that is very irregular or "wavy" will possess a foreshock region that emits electrons and a second connected region that collects these electrons. Based on our foot source location argument above, these collection points (featuring inflowing electrons with progressively increasing $v_\perp$) are then the Type II emission source regions. There is phenomenological evidence that the above-described scenario may occur. Specifically, *Reiner et al.* [1998] identified an isolated, very active Type II source region at the interception point of a CME and corotating interaction region (CIR). A shock is anticipated upstream of both structures and their intersection would create the same connected emitter/collector topology as the single "wavy" shock. Inflowing electrons from shock/shock interactions may also explain the Type II enhancements recently reported with merging CMEs [*Gopalswamy et al.*, 2001].

[31] While previous theories have emphasized Langmuir wave-wave interactions in the formation of IP Type II emission, our observations presented here in/near the Type II source region present significant challenges to these previous theories. For example, the wave-wave interaction theory cannot explain the ECH fine structure of the Type II emission. The frequency upshift of the emission and its broad bandwidth (many times the width of the Langmuir wave band) become increasingly difficult to explain as well.

[32] The ECH resonance condition predicts coupling of energetic foreshock electrons directly to the o-mode near wave frequencies $f \sim f_p \sim mf_c$ for $m \geq f_p/f_c$. The optimum coupling occurs when the wave phase velocities become small (near f_p), thereby allowing the waves to directly resonate with low energy suprathermal electrons. As explained by *Wu and Lee* [1979], retaining relativistic terms

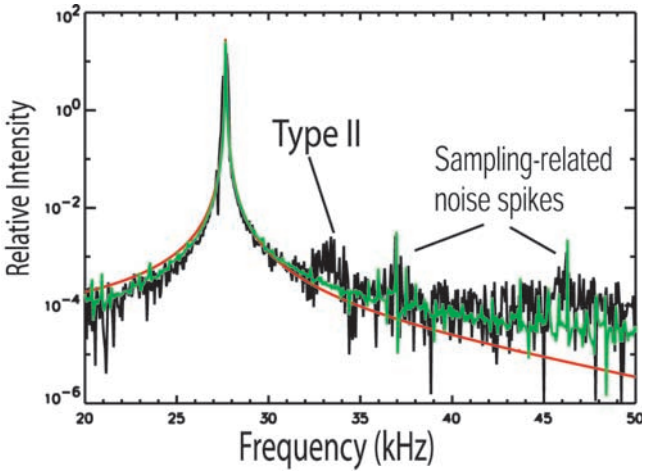

Figure A1. Fourier power spectrum of the measured TDS waveform (extension of Figure 3, in black), the spectrum of a sine wave at 27.8 kHz (red), and the spectrum of the same sine wave after undergoing the TDS digitization/intensity compression algorithm (green). Note that the observed spikes at 37 and 46 kHz are associated with the TDS-related digitization noise spikes while the Type II emission is associated with a relatively noise-free portion of the digitization process.

is important to keep at all energies, because the inclusion of the relativistic effects incorporates velocity dependencies that alter the non-relativistic formalism even at low energies. In our application, relativistic effects make the resonant velocity vary directly with index of refraction and retention of the relativistic terms makes the formalism consistent with Type II observations at the source.

Appendix A: Digitization Noise Analysis in TDS System

[33] The Wind/WAVES Time Domain Sampler (TDS) is an analog-to-log-digital waveform receiver designed to sample intense, bursty waveforms. Antenna differential voltage V_A is sampled and compared with a decaying RC circuit $V(t) = V_0 e^{-t/RC}$. When the signals are equal, $V_A = V(t_A)$, the time t_A is digitized and telemetered. The "logger" scheme gives roughly 90 dB of dynamic range in 8 bits but introduces noise to the power spectrum of the data. In particular, this nonlinearity introduces secondary spectral lines that appear at low intensities in the TDS spectra. We demonstrate here that the signals between 32 and 35 kHz in Figure 3 are not associated with the TDS digitization process.

[34] Figure A1 shows the Fourier power spectrum of the TDS waveform data, as in Figure 3, along with the spectrum of a pure large sine wave (indicated in red) with the same peak frequency and power as the intense Langmuir wave at 27.8 kHz. The green line indicates this same sine wave after going through the TDS data compression algorithm. As suggested by the display, the distinct, narrow spikes at 37 and 46 kHz appear to be associated with the TDS intensity compression process. There is no evidence in the model calculation of enhanced TDS digitization noise between 30 to 35 kHz. Thus the observed factor of ~10 rise in broadband emission at these frequencies (Type II emission) is apparently unrelated to the sampling system.

[35] There are two further arguments for the case of weak Type II emission between 32 and 35 kHz as observed in the TDS: First, the spikes are expected to be very narrowbanded (<1 kHz), mimicking their narrowband parent emission. However, the weak Type II emission is broadbanded, extending almost 3 kHz in width. The creation of a broadband emission via the nonlinear system is not expected. Second, the more sensitive thermal noise receiver (see Figure 2) also detected enhanced activity between 33 and 35 kHz at this time consistent with the observations in the TDS waveform system, indicating the signal is independnt of TDS noise generation.

Appendix B: Another Example of f_c Harmonic Structure

[36] Given the importance of the observation of ECH emissions in the Type II emission, other cases for such fine structure should be included to support the proposed theory. The difficulty is that the emission, away from its source, tends to be weak and thus below the sensitivity of the WIND Waves' Time Domain Sampler (TDS) waveform receiver. The *Bale et al.* [1999] case is a notable exception when the emission intensified near its source allowing detection in the TDS.

[37] However, upon further examination of the Waves data, a second case has recently been found. Specifically, on 21 October 2001, WIND passed through an IP shock that was also a probable type II source location. This shock passage occurred near 1640 UT. However, the type II emission remained relatively intense, being detectable in the TDS about 13 hours before the shock encounter. Thus observation of fine structure in the Type II could occur in a quiescent environment away from the shock, further reducing signal levels of other shock-related emissions in the TDS receiver.

[38] Figure A2 shows the WIND Waves thermal noise receiver at 1 min resolution in time and ~2 kHz resolution in frequency for the period of interest. Note that a rather broadband type-II emission is clearly evident near 40 kHz, with signal levels exceeding 10 dB above the background.

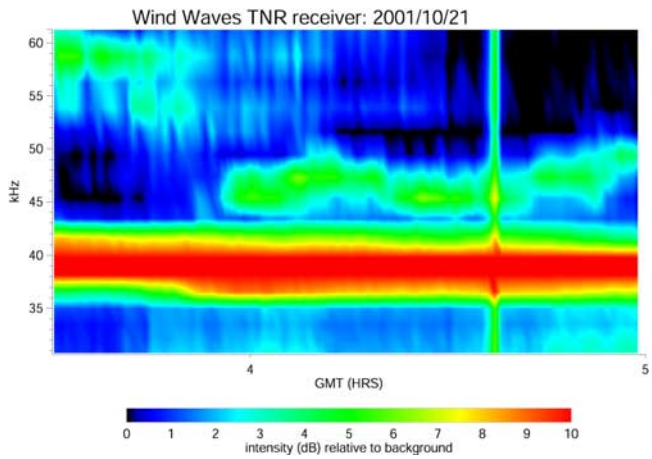

Figure A2. WIND Waves Thermal Noise Receiver (TNR) spectrogram showing an intense Type II emission about 12 hours before encounter with the Type II source/IP shock.

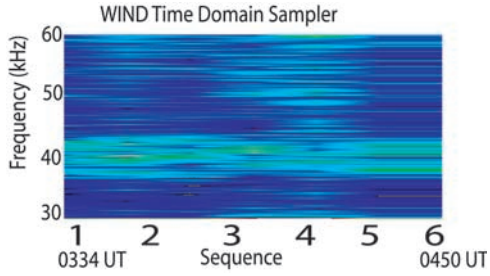

Figure A3. A sequence of six spectra taken from the WIND Waves Time Domain Sampler (TDS), capturing the same Type II event as that in Figure A2, but with ~100 Hz spectral resolution. The temporal resolution is poor (only six measurements in 80 min), which horizontally "stretches" the fine structure observed in frequency. This fine structure appears to be ECH emission with ~few hundred Hz separation.

[39] Between 0330 and 0500 UT, the TDS had six triggered waveform capture events like those in Figure 3 (120 kS/s in a ~17 ms window). These waveforms were Fourier Transformed and placed in sequence to form a high spectral resolution spectrogram, shown in Figure A3. Note that the spectrogram is aligned in TDS waveform sequence and not in exact time. Further, six temporal "slices" over a 90 min period is temporally poor resolution. However, the advantage of this approach is the extremely high spectral resolution, at about 100 Hz, along the y-axis. Comparing Figures A2 and A3, it is clear that fine structure is evident in Figure A3 that is essentially "smoothed over" in Figure A2. Further, this fine structure persists from sequence to sequence. The structure, at a few hundred Hz, is considered the electron cyclotron frequency at the Type II source. Its presence is consistent with the theory presented above.

[40] **Acknowledgments.** We thank Robert MacDowall for helpful comments regarding early versions of this manuscript.

[41] Shadia Rifai Habbal thanks Peter Yoon and another referee for their assistance in evaluating this paper.

References

Bale, S. D., et al. (1999), The source region of an interplanetary type II radio burst, *Geophys. Res. Lett.*, *26*, 1573.

Bougeret, J.-L., et al. (1995), WAVES: The radio and plasma wave investigation on the WIND spacecraft, *Space Sci. Rev.*, *71*, 231.

Cairns, I. H. (1986), Fine structure of plasma waves and radiation near the plasma frequency in the Earth's foreshock, *J. Geophys. Res.*, *91*, 2975.

Cane, H. V., R. G. Stone, J. Fainberg, R. T. Stewart, J.-L. Steinberg, and S. Hoang (1981), Radio evidence for shock acceleration of electrons in the solar corona, *Geophys. Res. Lett.*, *8*, 1285.

Farrell, W. M. (2001), Direct generation of o-mode emission in a dense, warm plasma: Applications to interplanetary Type II emissions and others in its class, *J. Geophys. Res.*, *106*, 15,701.

Fitzenteiter, R. J., J. D. Scudder, and A. J. Klimas (1990), Three-dimensional analytical model for the spatial variation of the foreshock electron distribution function: Systematics and comparisons with ISEE observations, *J. Geophys. Res.*, *95*, 4155.

Gopalswamy, N. S. Yashiro, M. L. Kaiser, R. A. Howard, and J.-L. Bougeret (2001), Radio signatures of coronal mass ejection interaction: Coronal mass ejection cannibalism?, *Astrophys. J.*, *548*, L91.

Lepping, R. P., et al. (1995), The Wind magnetic field investigation, *Space Sci. Rev.*, *71*, 207.

Lin, R. P., et al. (1995), A three-dimensional plasma and energetic particle investigation for the Wind spacecraft, *Space Sci. Rev.*, *71*, 125.

Nelson, G. J., and D. B. Melrose (1985), Type II bursts, in *Solar Radiophysics*, edited by D. J. McLean and N. R. Labrum, Cambridge Univ. Press, New York.

Reiner, M. J., et al. (1998), On the origin of radio emissions associated with the January 6–11, 1997, CME, *Geophys. Res. Lett.*, *25*, 2493.

Tidman, D. A. (1971), and N. A. Krall, *Shock Waves in Collisionless Plasmas*, John Wiley, New York.

Wu, C. S., and L. C. Lee (1979), A theory of terrestrial kilometric radiation, *Astrophys. J.*, *230*, 621.

S. D. Bale, Space Science Laboratory, University of California, Berkeley, Berkeley, CA 94720, USA.

J.-L. Bougeret, Departement de Recherche Spatiale, Observatoire de Paris, Meudon 97005, France.

M. D. Desch, W. M. Farrell, R. J. Fitzenreiter, and M. L. Kaiser, Laboratory for Extraterrestrial Physics, NASA Goddard Space Flight Center, Code 695, Greenbelt, MD 20771, USA. (william.farrell@gsfc.nasa.gov)

K. Goetz, School of Physics and Astronomy, University of Minnesota, Minneapolis, MN 55455, USA.